



X-ray methods to observe and quantify adhesive penetration into wood

Joseph E. Jakes^{1,*} , Charles R. Frihart¹ , Christopher G. Hunt¹ , Daniel J. Yelle¹ ,
Nayomi Z. Plaza¹ , Linda Lorenz¹ , Warren Grigsby² , Daniel J. Ching³ , Fred Kamke³ ,
Sophie-Charlotte Gleber⁴ , and Xianghui Xiao⁴ 

¹ Forest Biopolymers Science and Engineering, Forest Products Laboratory, USDA Forest Service, One Gifford Pinchot Drive, Madison, WI 53726, USA

² Scion, 49 Sala Street, Private Bag 3020, Rotorua 3046, New Zealand

³ Wood Science and Engineering, Oregon State University, 119 Richardson Hall, Corvallis, OR 97331, USA

⁴ Advanced Photon Source, Argonne National Laboratory, 9700 Cass Ave., Lemont, IL 60439, USA

Received: 23 June 2018

Accepted: 9 August 2018

Published online:

21 August 2018

© This is a U.S. government work and its text is not subject to copyright protection in the United States; however, its text may be subject to foreign copyright protection 2018

ABSTRACT

To accelerate development of new and improved wood adhesives for engineered wood products, the optimal adhesive penetration into wood needs to be better understood for specific products and applications. Adhesive penetration includes both flow of adhesives into wood micron-scale voids and infiltration into the polymer components of the wood cell wall layers. In this work, X-ray computed tomography (XCT) and X-ray fluorescence microscopy (XFM) were used to study adhesive flow and infiltration. Model wood–adhesive bondlines were made using loblolly pine (*Pinus taeda*) latewood substrates and bromine-substituted phenol formaldehyde (BrPF) resins with different weight-average molecular weights (M_w). The Br substitution facilitated both qualitative and quantitative observations using XCT and XFM. The BrPF resin flow into wood was visualized using XCT volume reconstructions and quantified by calculating the weighted penetration (WP). Examination of the shape of the cured BrPF–air interface in longitudinal tracheid lumina revealed that capillary action often played a role in BrPF flow. XFM mapping revealed the pathways of BrPF infiltration into the wood cell walls, and the results were used to calculate BrPF cell wall weight percent gain (WPG_{CW}) in individual wood cell walls. Both WP and WPG_{CW} decreased with increasing BrPF M_w . Additionally, the middle lamella had higher WPG_{CW} than its neighboring secondary cell walls, and within a given bondline the WPG_{CW} decreased with increasing distance of the cell from the bondline. The results provide new insights that are needed in the development of improved models to understand and predict wood–adhesive bondline performance.

Address correspondence to E-mail: jjakes@fs.fed.us

Introduction

Adhesives play an indispensable role in the manufacture of many modern engineered wood products such as plywood, oriented strandboard, laminated veneer lumber, and cross-laminated timbers. However, the development of new and improved wood adhesives is hindered by an incomplete mechanistic understanding of the performance of wood–adhesive bondlines in these products. Wood adhesives are currently developed empirically for specific products and end uses, often utilizing standardized tests (e.g., ASTM D905 and D2559 [1]) that are designed to assess the overall performance of bonded assemblies and the final product. This development process is inefficient where new testing is often needed for changes made to any of the dozens of variables associated with the adhesive, wood, bonding processes, and service life that can affect bondline performance [2, 3]. Improved models capable of predicting the performance of adhesive bondlines, as process variables change, should accelerate efforts to develop new and improved adhesives.

The complexity of wood–adhesive interactions makes studying bondlines difficult. Although bondline properties are more of a continuum than discrete links, the Marra chain-link analogy (Fig. 1) aids researchers by dividing the bondline into components for individual study [4]. Moving from the

middle of the bondline into a wood substrate, the links consist of the bulk adhesive (pure adhesive not affected by the presence of wood substrates), adhesive interphase (adhesive affected by the presence of wood substrate), interface (boundary between wood and adhesive), wood interphase (wood modified by the surface preparation or adhesive), and the bulk wood (unmodified wood). Generally, a wood adhesive is considered satisfactory if the bondline transfers sufficient loads between wood substrates, and if failure does occur, it occurs in the bulk wood. Bondline strength and amount of wood failure are what standardized tests are designed to evaluate [1]. Arguably, it is not well understood why some adhesives work better than others. For example, although exterior-grade wood adhesives are available and provide superior bond durability [5–7], the mechanisms by which these adhesives bond to wood are not well understood. This lack of understanding is especially notable when the end use includes fluctuations in moisture content, requiring the bondline to be capable of withstanding dimensional changes caused by both the wood and the adhesive absorbing and desorbing water [8, 9].

An improved understanding of adhesive penetration in the wood interphase link (Fig. 1) has been identified as a key to developing new and improved wood adhesives, especially for moisture durability [3, 5]. It has been proposed that adhesive in the wood interphase can repair cells on the wood surface damaged during surface preparation and, through this reinforcement, mechanically stabilize the wood near the bondline [10]. Adhesive penetration occurs at multiple levels of scale, ranging from molecular level to macroscale, and in this paper will be discussed using the terms flow and infiltration to distinguish two different scales [5]. Flow is the movement of adhesives across a wood surface and into micron-size voids that may include anatomical features (lumina, rays, pits, resin canals) and cracks formed during surface preparation or drying. Generally speaking, flow affects mechanical interlocking and the amount of area in the interface links where chemical bonds between the adhesive and wood surfaces contribute to the mechanical integrity of the bond [11, 12]. Infiltration occurs when adhesive components enter the cell wall material and interact at the molecular scale with wood cell wall polymers. Infiltration affects the chemical interactions between wood polymers and adhesive components in cell

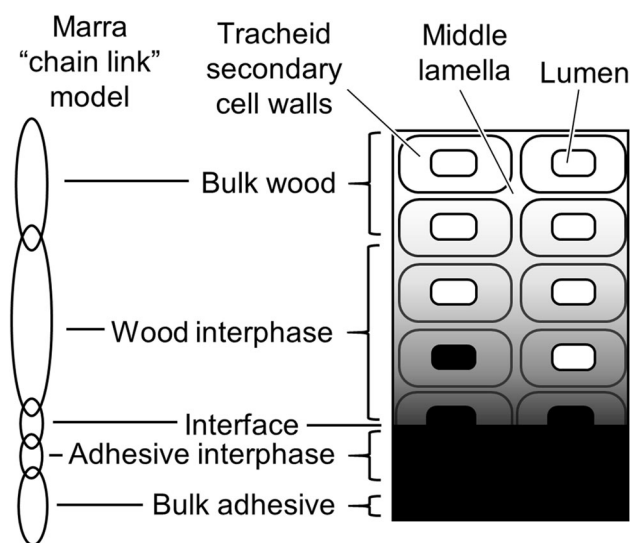


Figure 1 Marra chain-link model [4] for a wood adhesive bondline together with a cellular-scale schematic of a wood adhesive bondline.

walls, which can modify the cell wall physical properties (for example, swelling and mechanical) in the wood interphase [13–15].

A prerequisite to identifying what makes a good wood interphase link is developing the necessary tools to observe and quantify both adhesive flow and infiltration into wood. In 2007, Kamke and Lee [3] provided a thorough review of techniques that have been employed to study flow (optical microscopy, electron microscopy, and X-ray computed tomography (XCT)) and infiltration (optical microscopy, energy-dispersive X-ray spectroscopy, nanoindentation, ultraviolet photometer microscopy, neutron activation, autoradiography, and X-ray spectromicroscopy). More recently, scanning thermal microscopy [16, 17], confocal laser scanning microscopy [18–21], atomic force microscope infrared spectroscopy [22], X-ray fluorescence microscopy (XFM) [23, 24], and small-angle neutron scattering [25, 26] have also been employed to study infiltration. Despite this previous work, there are still many unanswered questions about how adhesives penetrate wood and how to quantify adhesive flow and infiltration into wood.

In this paper, we combine high-resolution XCT and XFM techniques to study adhesive flow and infiltration into the wood substrates of six model bondlines made using loblolly pine (*Pinus taeda*) latewood and six different brominated phenol formaldehyde (BrPF) resins with different weight-average molecular weight (M_w). X-ray computed tomography is a non-destructive technique that can be used to quantify the extent of adhesive flow into the wood structure and create three-dimensional (3D) visualizations of adhesive flow into wood [27, 28]. X-ray fluorescence microscopy is a technique capable of mapping and quantifying adhesive flow into wood structure and infiltration into wood cell walls [23, 24]. In this work, the Br substitution assisted both XCT and XFM analyses. Because both solubility parameters and molecular size influence infiltration [29, 30], the Br substitution may have modified the penetration behaviors with respect to unsubstituted phenol formaldehyde (PF) resins. However, the model BrPF bondlines were still useful to gain new insights into how adhesives interact with wood in the wood interphase link.

Materials and methods

Full experimental details of the BrPF resin and bondlines prepared with the resin and latewood loblolly pine are given by Jakes et al. [24]. Briefly, phenol was replaced with 3-bromophenol in the resin formulation, resulting in a resin with the structure shown in Fig. 2. Aliquots of BrPF were removed at 45, 85, 115, 135, 155, and 175 min after commencement of the condensation stage of the resin manufacture. Although not measured quantitatively, BrPF viscosity and M_w were observed to increase with time in this condensation stage. Separate bondlines were made using each resin aliquot and will be referred to by their time in the condensation stage of the reaction (45-min, 85-min, etc.). For the wood substrates, pristine tangential–longitudinal surfaces in latewood loblolly pine were prepared using a disposable microtome blade in a sledge microtome. Each substrate measured approximately 10 mm longitudinal \times 5 mm tangential \times 10 mm radial. Bondlines were made by applying enough BrPF resin to the pristine surfaces of two substrates to ensure abundant resin squeeze-out. After 5-min open assembly time, two substrates were clamped together using an office binder clip. After an additional 5 min, the assemblies were placed in a 155 °C oven and cured in situ for 45 min.

X-ray computed tomography

For XCT, a specimen with a rectangular cross section between 1 and 2 mm on a side and with a length of about 10 mm was cut from each of the six loblolly pine BrPF bondlines. The bondline was centered in the cross section of the XCT specimen, and the longitudinal wood axis was aligned along the length. Phase-contrast imaging was performed at beamline 2-BM-B at the Advanced Photon Source at Argonne National Laboratory (Argonne, IL, USA) using a filtered polychromatic X-ray illumination beam with

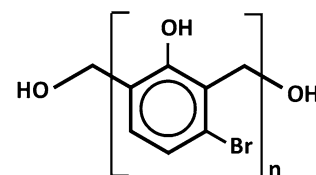


Figure 2 Molecular structure of brominated phenol formaldehyde (BrPF) resin.

peak energy of 27 keV. The X-ray beam hit on a lutetium aluminum garnet scintillator screen that was used to convert the X-rays into visible light. The converted visible light projections were collected using a PCO (Kelheim, Germany) Dimax camera with a $10 \times$ Mitutoyo (Kawasaki, Japan) long-working distance microscope objective lens. The setup allowed a 2.2×2.2 mm field of view. A full tomographic dataset consisted of 1500 projections collected evenly over a 180° rotation with 5-ms exposure time for each projection. Tomograms were reconstructed using Tomopy [31]. Tomogram resolution was $1.1 \mu\text{m}$ per voxel side length. Volumes from the middle 1200 slices (1.32 mm) from the bondline were used for further analysis.

The tomograms were segmented into the four phases BrPF, BrPF–wood mixture, wood, and air using an analysis based on previously established protocols for segmentation of wood–adhesive bondlines [28, 32]. Briefly, a Gaussian mixture model was fit to pixel intensity profiles. Based on the expected order of intensity, peaks were assigned to the five phases, in order of decreasing intensity: BrPF, BrPF–wood mixture, wood, air, and phase-contrast shadows. The phase-contrast shadow phase was merged with the air phase. Within a two-dimensional XCT cross section slice, areas of BrPF–wood mixture were kept only if the area encompassed by the BrPF–wood mixture and adjacent BrPF exceeded 100 pixels. If the area did not exceed 100 pixels, the BrPF–wood mixture pixels were assigned to the cell wall phase. Similarly, if an area of cell wall phase did not exceed 100 pixels, that area was assigned to the air phase. This size filtering was done to reduce noise. To calculate bondline distances, the bondline was first located by marking it with a scattering of points throughout the volume; then, these points were used to calculate a best-fit plane. This best-fit plane was used to calculate the volume fraction of BrPF voxels on either side of the bondline as a function of bondline distance. In this calculation, the positive and negative sides of the bondline were randomly assigned. Additionally, to maintain consistency between the bondlines, the BrPF volume fraction was only quantified within a $500 \mu\text{m}$ distance from the bondline. The BrPF volumes were then used to calculate the adhesive weighted penetration (WP) [28], defined as

$$\text{WP} = \sqrt{\frac{\sum Y_i^2 A_i}{\sum A_i}}, \quad (1)$$

where A_i is the area or volume of an adhesive particle and Y_i is the perpendicular distance from the bondline to the A_i centroid. For each bondline, WP was calculated for each substrate separately and for both substrates together. Three-dimensional BrPF volume reconstructions and visualizations were created using the 3D Viewer plugin [33] in FIJI [34]. A 3D Gaussian blur filter [sigma (radius) = 2] was applied to improve the visual appearance of the rendered BrPF adhesive volumes.

X-ray fluorescence microscopy (XFM)

XFM mapping was performed on sections prepared from the 45-, 85-, 115-, 135-, and 155-min bondlines. These were the same sample sections prepared for our previous work, with full preparation details given by Jakes et al. [24]. Briefly, $2\text{-}\mu\text{m}$ -thick transverse sections of the bondlines were cut using a diamond knife fitted into a Sorvall (Norwalk, Connecticut, USA) MT-2 ultramicrotome. The sections were clamped in a copper StrataTekTM 1/1 mm double-folding hole TEM grid obtained from Ted Pella, Inc. (Redding, California, USA). The sides of the folded TEM grids were then taped to the APS 2-ID-E beamline aluminum stick sample holder. For each BrPF condensation time, one section was prepared and imaged. XFM imaging was performed at APS beamline 2-ID-E using a 15.0 keV incident beam energy. Two beamline configurations were used. In the first configuration, the beam was focused with a high-flux zone plate objective (100 nm outermost zone width, $320 \mu\text{m}$ diameter) to a spot size of $0.8 \mu\text{m}$ by $0.5 \mu\text{m}$ full width at half maximum in the vertical and horizontal directions, respectively. Images were created using raster scanning and $0.3\text{-}\mu\text{m}$ steps with a 5-ms dwell time at each step. In the second configuration, the beam was focused with a high-resolution zone plate objective (100 nm outermost zone width, $160 \mu\text{m}$ diameter) to a spot size of $0.28 \mu\text{m}$ by $0.28 \mu\text{m}$ full width at half maximum and images were created using $0.15\text{-}\mu\text{m}$ steps with 20-ms dwell times. Data analysis and Br quantification were carried out using the MAPS software package [35]. In brief, the full spectra were fit to modified Gaussian peaks, the background was iteratively calculated and subtracted, and the results were compared to standard reference materials (RF8-200-S2453, AXO GmbH, Dresden).

Results and discussion

X-ray computed tomography (XCT)

An example tomogram of a transverse plane from the 135-min BrPF bondline is shown in Fig. 3a. Similar to previous work using electron-rich atoms like Br and I in adhesive formulations for XCT studies [28, 36], the added electron density of the Br increased the X-ray attenuation of the BrPF resin component. The increased attenuation made the BrPF appear brighter (white) and distinguishable from the wood cell walls (lighter gray) and air (dark gray to black). The substrates for these bondlines were prepared by bonding nominally tangential–longitudinal surfaces. In this orientation, the rays were oriented normal to the plane of bondlines. As shown in Fig. 3a, the BrPF resin flowed into the lumina of some of the rays and longitudinal tracheid near the prepared surfaces. Using the contrast provided by the increased attenuation of the BrPF, the tomogram in Fig. 3a was segmented into the four phases, BrPF, BrPF–wood mixture, wood, and air, as shown in Fig. 3b. By

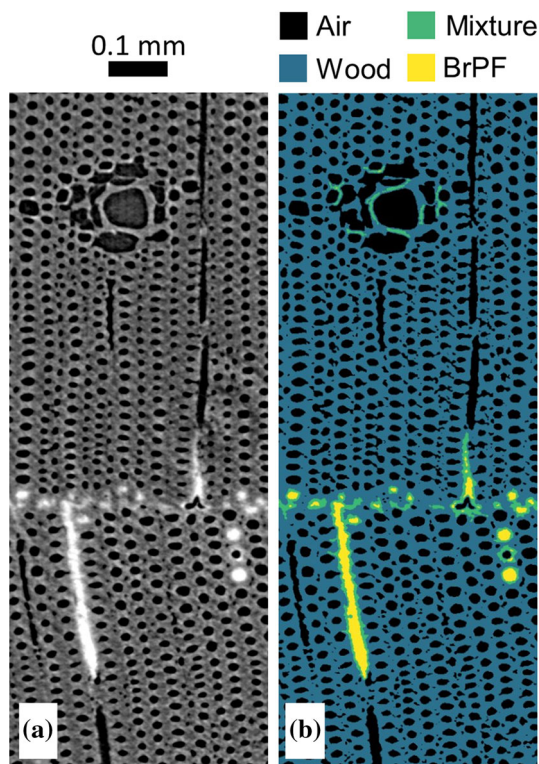


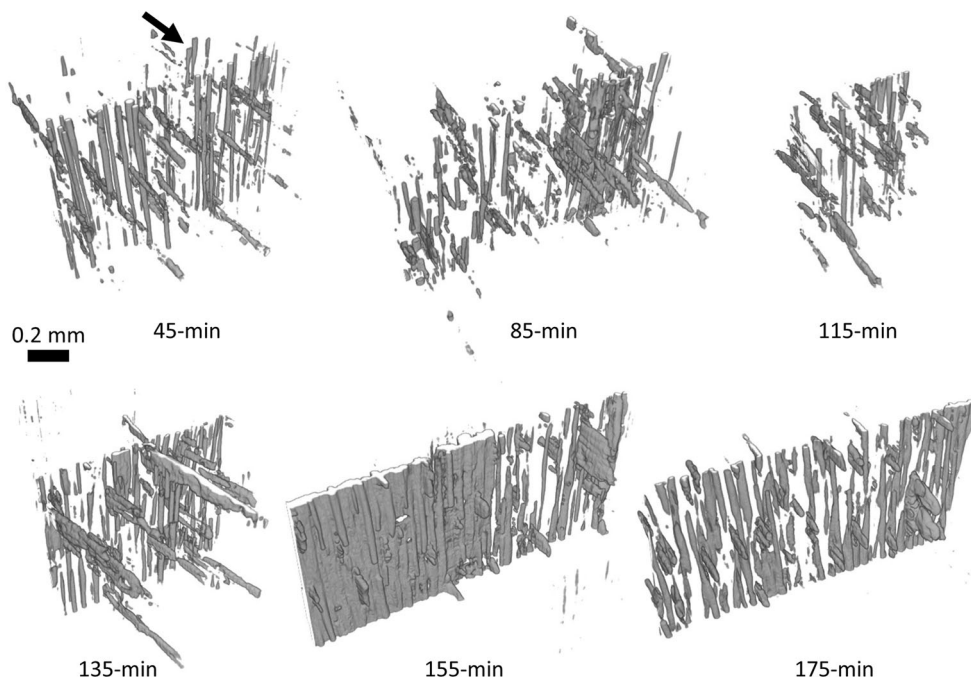
Figure 3 X-ray computed tomography (XCT) slice showing a bondline made using latewood loblolly pine and the 135-min BrPF resin **a** before and **b** after segmentation.

definition, the BrPF–wood mixture phase was defined as voxels with intensities intermediate to BrPF and wood cell walls. However, owing to uncertainty in the composition of the BrPF–wood mixture voxels (for example, the voxels may include wood cell walls infiltrated with BrPF or a material interface) and some phase-contrast edge effects in thin-walled cells [37] (for example, see the thin-walled cells near the resin canal at the top of the tomograms in Fig. 3 that segmented into the BrPF–wood mixture phase), this mixed phase was not included in the 3D visualizations of the BrPF or in the quantification of BrPF flow into the wood. X-ray fluorescence microscopy will later be shown to be more capable than XCT to observe the infiltration of BrPF into the wood cell walls.

Representative volumes of the segmented BrPF from each bondline are shown in Fig. 4. The flow of BrPF resin into longitudinal tracheid lumina and ray cells accessible at the prepared surface was readily observed. Moreover, BrPF was also observed to flow through rays and then pits into longitudinal tracheids away from the bondline (for example, see the arrow in the 45-min reconstructions in Fig. 4). The 45-, 85-, 115-, and 135-min bondlines had substantially greater BrPF flow than the 155- and 175-min bondlines. The higher M_w of the BrPF resin in the 155- and 175-min bondlines likely limited the extent of BrPF flow. Also, in this series, most of the bondlines lacked any distinct bondline. It is possible that the resin layer present was too small for the 1.1 μm XCT resolution or segmentation criteria to capture, as has been suggested previously based on comparisons of fluorescence microscopy and XCT of bondlines [28]. Or it may have been too easy for the resin to squeeze out because the bond area was small and the surfaces of the high-density latewood were microtomed flat. The 155-min bondline perhaps provides an exception as the left-hand side of the bondline in Fig. 4 was much thicker. We suspect that the binder clip used to clamp the bondline may not have been centered on the 155-min specimen and the pressure was predominantly applied to the right side of the bondline, which had a much thinner bondline and greater flow into the rays prior to curing.

Adhesive flow into the wood structure occurs via adhesive wetting and hydrodynamic forces [2, 3]. In forming the BrPF bondline, wetting forces were expected to dominate during the initial application of the resin and open assembly time when

Figure 4 X-ray computed tomography (XCT) volume reconstructions of BrPF resins in bondlines. The arrow in the 45-min reconstruction indicates a tracheid lumen filled away from the bondline. Full reconstructions and rotating movies are provided in the Online Resources.



hydrodynamic forces were absent. During the closed assembly time, clamping hydrodynamic forces developed and likely caused additional adhesive penetration. The shape of the BrPF–air interface inside longitudinal tracheid lumina provided insights into which forces were contributing in the final increment of flow through a lumen before cure. In a small tube, like a lumen, the wetting of a liquid onto the inner surface can cause the liquid to be pulled up the sides of the tube as the result of capillary action. Such behavior was almost always identified in the BrPF flow in longitudinal tracheid lumina by

observing the concave meniscus of the BrPF–air interface inside of lumina (Fig. 5a). The observation that most BrPF in lumina showed the resin being pulled up the lumen surfaces suggested that even after clamping, some additional capillary flow occurred. However, a convex meniscus (Fig. 5b) of the BrPF–air interface was observed in a few lumina in the 155-min and 175-min bondlines. The convex shape is indicative of flow dominated by hydrodynamic forces. It is likely that in the longitudinal tracheid shown in Fig. 5b, the resin had cured to the point where the attractive forces between the higher M_W BrPF molecules were greater than the attractive forces along the lumen surfaces. This is consistent with the known relationship that the wettability of PF on a wood surface decreases with increasing PF M_W [38]. Practically, these hydrodynamic forces from the clamping pressure forced the resin through the lumina, and with flow near the lumen surfaces restricted, a convex meniscus formed.

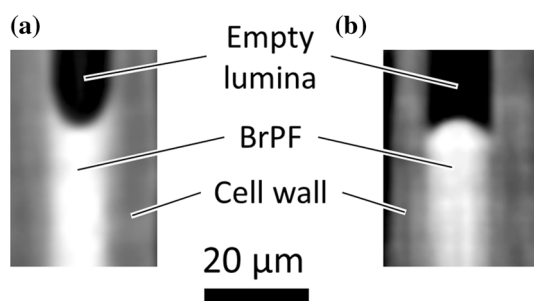


Figure 5 X-ray computed tomography (XCT) images of planes along the longitudinal tracheid axis showing **a** a concave BrPF meniscus and **b** a convex BrPF meniscus, which are characteristic of capillary and hydrodynamic forces, respectively, acting on the BrPF resin during the final increment of flow through a lumen. The image in (a) is from the 85-min specimen and (b) is from the 155-min specimen.

In addition to qualitative observations of resin flow into a wood substrate, another goal of applying the XCT technique was to quantify the flow. As a first step, the flow of BrPF into the wood structure was quantified by calculating the volume fraction of BrPF voxels as a function of distance from the bondline, as plotted in Fig. 6. For reference, the approximate diameter of a longitudinal tracheid in the radial directions was 20 μm , and the average air volume

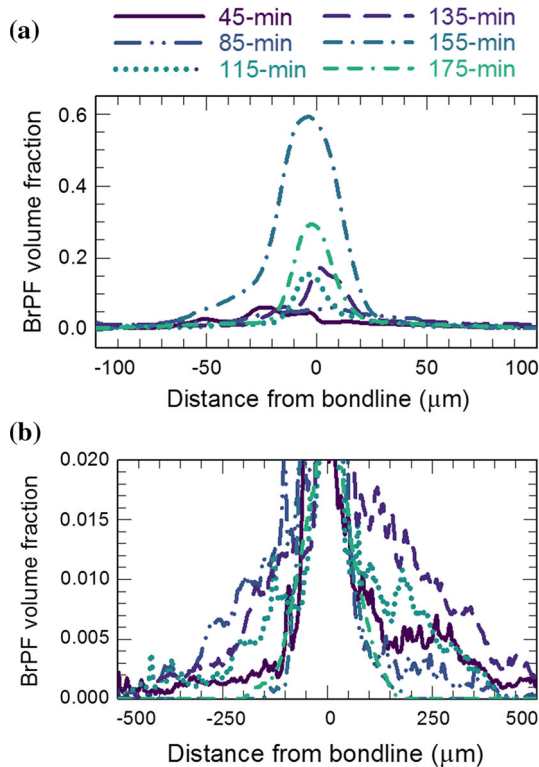


Figure 6 BrPF volume fraction as a function of distance from the bondline scaled to emphasize **a** the higher volume fraction nearest the bondline and **b** the lower volume fraction far from the bondline. The positive and negative substrate sides were randomly assigned.

fraction for latewood without BrPF was about 0.35. In the space nearest the bondline, Fig. 6a shows that BrPF resin with higher condensation time has a higher BrPF volume fraction. Moreover, despite the lack of obvious bondlines in the volume reconstructions (Fig. 4), the higher M_w BrPF had higher volume fractions near the adhesive link. However, the 45- and 85-min bondlines did not exhibit a defined volume fraction peak at the bondline. This is usually referred to as a “starved” bondline. In this case, it was likely that the relatively lower viscosity of BrPF in the 45- and 85-min bondlines allowed more resin to be moved away from the bondline by squeeze-out or capillary forces, resulting in less resin near the bondline compared to the higher M_w resins. In Fig. 6b, it can be observed that the 155- and 175-min bondlines go to nearly zero volume fraction at about 200 μm distance from the bondline, whereas the other bondlines show flow to greater distances. This agrees with the qualitative observations of shallower ray penetration in the 155- and 175-min bondlines in

Fig. 4 and the larger role of viscosity relative to capillary forces in the 155- and 175-min specimens.

In this study, even with our careful substrate preparations, the BrPF distributions in Fig. 6 were not always symmetric with differences observed between the two sides of bondline specimens. Even though the top and bottom substrates during bondline preparation were not recorded, so potential gravity effects on resin penetration could not be evaluated, differences beyond potential gravity effects were observed. For example, the 45-min specimen showed more flow into the negative side at distances less than 50 μm , and more flow into the positive side at distances greater than 150 μm . This suggests that even for model bondlines, substantial variations are to be expected. While the anatomical wood orientation with respect to the bondline surface is known to affect adhesive flow, we attempted to control the orientation by preparing nominally tangential–longitudinal surfaces for bonding. Paris and Kamke observed how the slope of grain with respect to the bonding surface can affect adhesive flow into the lumina near the bondline [28]. Measurements made using the XCT tomograms and FIJI [34] revealed that all the surfaces in this study were within 2° of the longitudinal wood axis. Hass and coworkers also showed that ray orientation with respect to the bonding surface can affect adhesive flow [39]. Here, ray orientation was checked by measuring their angles with the bondline in transverse plane tomograms. All the angles were within 3° of perpendicular to the bondline except for the negative distance sides of the 135- and 155-min specimens in Fig. 6, which were 15° and 10° from perpendicular, respectively. However, any ray misalignment in these two substrates did not have an observable effect on volume fraction of BrPF as a function of distance from the bondline.

Ultimately, researchers desire a single parameter to quantify adhesive flow into wood that can be correlated to measured bulk bondline properties such as strength and amount of wood failure. It has been well documented that only looking at a single two-dimensional plane, either extracted from an XCT dataset or obtained by some other type of microscopy, gives an incomplete assessment of adhesive penetration because adhesive flow can vary substantially along a bondline [39]. Three-dimensional XCT data are promising because flow can be averaged along a bondline. One method to parameterize

adhesive flow is simply measuring the maximum penetration depth into the wood substrate. However, the randomness of wood structure, especially in hardwoods with their vessel elements, makes this parameter ineffective as a metric of adhesive flow [3, 28]. Other proposed methods include calculating effective penetration (EP) [40] and weighted penetration (WP) [28]. Paris and Kamke determined WP to be better than EP to characterize adhesive penetration because EP is simply a measure of total adhesive area divided by bondline length, and distance away from the bondline is not part of the EP calculation [28]. In contrast, WP accounts for both amount of adhesive flow and distance away from the bondline. In Fig. 7, WP is calculated using the BrPF phase for each individual substrate and both substrates together. The lower WP values for the 155- and 175-min bondlines agree with the observations made from the BrPF volume reconstructions (Fig. 4) and volume fraction distributions (Fig. 6) that these bondlines did not have as much flow into the substrates as the other bondlines.

In reviewing the results of this study and recent progress elsewhere, there are still issues that must be addressed to fully realize the potential of parameters like WP to quantify adhesive flow. For example, consider comparisons between the positive and negative sides of the 45-min bondline BrPF volume fraction distribution (Fig. 6) and their calculated WP values (Fig. 7). In this case, despite observing more flow into the negative side for distances less than 50 μm , the positive side of the bondline had a higher

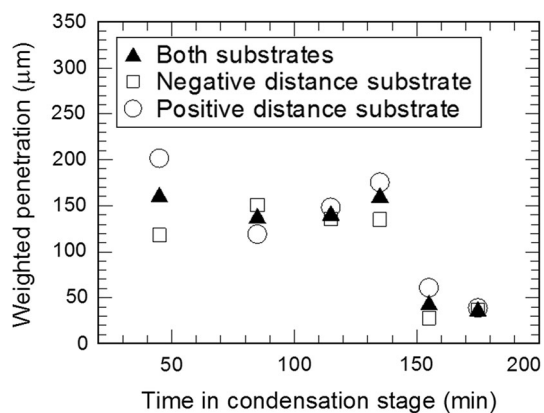


Figure 7 Weighted penetration (WP) calculations using Eq. 1 for each bondline as a function of time in the condensation stage for the BrPF used to make the bondline. The negative and positive distances refer to the side of the BrPF volume fraction distribution in Fig. 6.

WP because it had more flow for distances greater than 150 μm . Moreover, with respect to bondline performance, adhesive far from the bondline or in isolated adhesive pockets likely has little value [39]. This may imply that WP does not directly relate to bond performance because it does not measure adhesive connectivity. Resin canals and microcracks in the wood substrates could also overly influence WP quantification. Furthermore, imperfections in adhesive links, such as observed cracks in some bulk adhesive links of bondlines [39], are not accounted for despite their potentially large effects on bondline structural integrity. Another issue is that WP calculation requires segmentation of the resin phase, which for XCT required labeling the resin with a heavy atom. This labeling with bromine also likely affected both the final cross-linked PF network and resin–wood interactions. Ideally, a method is needed to quantify adhesive flow that does not require tagging or segmentation.

X-ray fluorescence microscopy (XFM)

The Br XFM maps of transverse sections from bondlines are shown in Fig. 8. The Br intensity could be used to observe resin penetration into wood because Br was covalently bonded to the BrPF resin monomer. However, even with this approach, we estimated that up to 1% of the Br may have detached during the resin manufacture and bonding because of the labile C–Br bond [24]. Therefore, it was decided that cell walls with intensities less than 2 $\mu\text{g}/\text{cm}^2$ would be considered background levels without resin infiltration [24]. In Fig. 8, the color intensity is on a log scale, and this background Br is useful to visualize the wood cellular structure.

Observations of flow into the wood structure from the XFM maps (Fig. 8) were consistent with those observed using XCT (Figs. 4, 6), with greater BrPF penetration for lower condensation times. The wood substrates for these model bondlines were prepared such that the rays were oriented normal to the bondline. Unfortunately, when 2- μm -thick transverse sections were prepared, they often broke along the ray cells. For example, see the right lower half of the 45-min section in Fig. 8. The increased Br intensity along this side indicated that the BrPF had flowed through this ray. This section also happened to cut through pits between this ray and its neighboring longitudinal tracheids. In the pit indicated by an

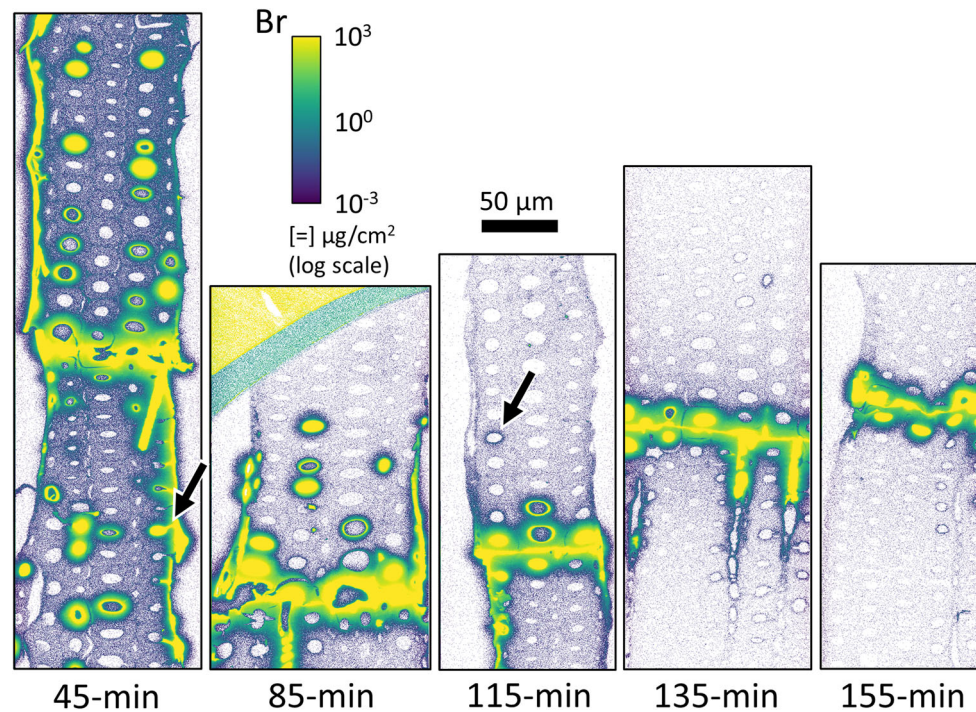


Figure 8 X-ray fluorescence microscopy (XFM) Br maps of transverse sections cut from BrPF bondlines. The maps were obtained using the high-flux zone plate beamline configuration (0.3- μm steps with 5-ms dwell times). The bondline in each section is positioned horizontally. The feature in the upper left-hand corner of the 85-min image is part of the copper grid holding

arrow in the 45-min section in Fig. 8, the resin flowed through the pit and filled the longitudinal tracheid lumen. In other pits along this ray, the resin entered the pits but did not flow into the connected longitudinal tracheids. Longitudinal tracheid lumina in the 45-min and 85-min sections that were multiple cells away from the bondline were also filled, which likely occurred through rays outside of the plane of the section as could be observed in the XCT results (Fig. 4). Some of the longitudinal tracheid lumina were also partially filled with evenly coated lumen surfaces, consistent with resin moving up a lumen with capillary action, such as the longitudinal tracheid lumina in Fig. 5a.

An advantage of XFM over XCT was the ability to clearly observe BrPF infiltration into the cell walls. BrPF infiltration can be observed in cell walls near the applied surface as well as in cell walls near the longitudinal tracheid lumina, ray cells, and pits through which the BrPF flowed. Additionally, distinct bondline links could be more easily observed in the XFM Br maps than the XCT results, especially for the 115-,

the section. In the 45-min section, the arrow indicates a pit connecting a ray to a longitudinal tracheid through which BrPF flowed. The arrow in the 115-min section indicates a tracheid with concentric BrPF infiltration, but without observable BrPF flow in the lumen.

135-, and 155-min bondlines. This is consistent with the peaks in the BrPF volume fraction plots in Fig. 6a. For these bondlines, the amount of infiltration within a cell wall layer decreased with increasing distance from where the infiltration initiated. Infiltration into the cell walls of longitudinal tracheids with BrPF in their lumina was also concentric, meaning that the amount of infiltration depended only on distance from the lumen surface. Furthermore, for some longitudinal tracheids without obvious BrPF in the lumen, there was concentric infiltration evident. For example, see the longitudinal tracheid indicated by the arrow in the 115-min section in Fig. 8. This suggests that during capillary flow of the BrPF through a lumen, there may have been a small amount of cell wall infiltration preceding the BrPF flow through the lumen.

The Br intensity could also be used to estimate the BrPF weight percentage gain of cell walls (WPG_{CW}) because the sections had well-defined 2 μm thickness and were thin enough for the X-ray beam to completely penetrate. The WPG_{CW} is different than the

typical bulk wood weight percentage gain reported in the wood modification literature because the bulk value also includes the mass of chemicals present in the lumina, rays, and pits. The WPG_{CW} was calculated using the resin molecular structure (Fig. 2) to estimate the mass of the BrPF segment associated with each Br. The mass of a BrPF segment associated with each Br depends on the number of repeating units. Each repeat unit (C_7H_7BrO) has one Br atom and a molar mass of 187.0 g/mol. However, a monomer ($C_8H_9BrO_3$) would also have one Br atom but a molar mass of 233.1 g/mol. Here, we assumed an average BrPF segment molar mass of 200.0 g/mol for each Br. By dividing the 200.0 g/mol BrPF segment molar mass by the 79.9 g/mol Br molar mass, 2.5 μg of BrPF per μg of Br was estimated. The XFM Br intensity was quantified in units of $\mu\text{g}/\text{cm}^2$, which were converted to WPG_{CW} per Eq. 2 using the section thickness ($2\ \mu\text{m} = 0.0002\ \text{cm}$) and assumed cell wall density ($1.5\ \text{g}/\text{cm}^3$).

$$WPG_{CW} = \left(\frac{\mu\text{g Br}}{\text{cm}^2} \right) \left(\frac{1}{0.0002\ \text{cm}} \right) \left(\frac{\text{cm}^3}{1.5\ \text{g cell wall}} \right) \left(\frac{2.5\ \mu\text{g BrPF}}{\mu\text{g Br}} \right) \left(\frac{1\ \text{g BrPF}}{1 \times 10^6\ \mu\text{g BrPF}} \right) (100). \quad (2)$$

Maps of the calculated WPG_{CW} of bondlines are shown in Fig. 9. In considering the infiltration of PF resins without Br substitution, it should be noted that for the same number of molecular PF segments, the WPG_{CW} would be about one half of those reported here for BrPF, as almost half the molar mass of the BrPF results from the Br.

The XFM maps revealed differences in cell wall BrPF infiltration across and within the different specimens. The amount of infiltration in the cell walls nearest the bondlines decreased with increasing condensation times. The estimated BrPF WPG_{CW} in the cell walls next to the bondline was about 20% in the 45-min specimen, with values closer to 8% in the 85-min and 135-min specimens, and 5% in the 155-min specimen. This dependence was likely because cell wall infiltration depends on the M_W of the infiltrating molecule [41, 42], and the BrPF M_W increased with condensation time. Moreover, even within the same specimen section the amount of infiltration varied in different longitudinal tracheids, especially as the distance from the bondline increased. For example, in the 85-min section (Fig. 9)

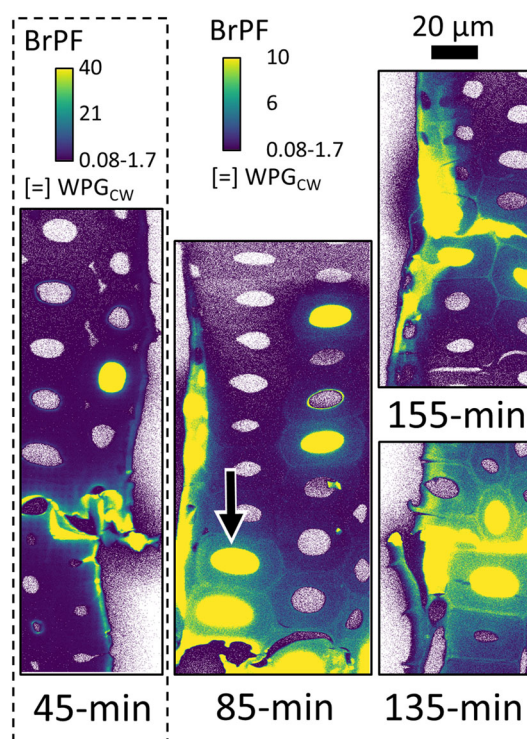


Figure 9 Close-up X-ray fluorescence microscopy (XFM) Br maps of transverse sections cut from BrPF bondlines. The maps were obtained using the high spatial resolution zone plate beamline configuration (0.15- μm steps with 20-ms dwell times). The color intensities are the WPG_{CW} of the BrPF infiltrated into the cell walls calculated using Eq. 2. Note that the brightest intensities include solid BrPF inside of longitudinal tracheid lumina and in the adhesive links. The intensity of this solid BrPF does not have meaning in the context of WPG_{CW} . The lowest color in the intensity calibration bar includes all pixels with background level Br intensities ranging from 0.1 to 2 $\mu\text{g}/\text{cm}^2$ (0.08–1.7 WPG_{CW}). Including this intensity range for the lowest color facilitated visualization of the wood cell walls in the Br maps.

the filled lumen in the lower left-hand corner exhibits at least twice as much infiltration as the filled lumen in the upper right-hand corner, which is the seventh longitudinal tracheid from the bondline. In this case, the resin likely traveled through a ray and then a pit into this longitudinal tracheid far from the bondline. By the time the resin reached this longitudinal tracheid, the low M_W component had probably either already infiltrated into cell walls along the flow pathway [43], or reacted with other BrPF molecules to increase the M_W . The remaining higher M_W BrPF could not infiltrate the cell wall as much as its lower M_W counterpart. Additionally, the alkali and water components of the resin also may have migrated out

of the resin, so that these resin components were not as available to swell the wood cell wall to facilitate the infiltration of BrPF in the longitudinal tracheid away from the bondline.

As infiltration is needed for an adhesive to modify cell wall properties [13–15], the observed differences in BrPF infiltration between and within sections indicate that simply observing lumen modification does not necessarily signify similar extents of cell wall infiltration and modification. It is well known in bulk wood treatments that lower M_W PF are more effective than higher M_W PF at increasing the dimensional stability of the treated wood [15, 44, 45]. This together with the current XFM findings suggests that in the lower M_W PF treatments, the increased stability arises from an increased WPG_{CW} . In future work, XFM and substituted PF can be used to better correlate WPG_{CW} with dimensional stability, which would inform researchers of the optimal levels of infiltration needed for cell wall stabilization.

The high spatial resolution of XFM also allowed observations of BrPF infiltration in individual cell wall layers, specifically secondary cell wall layers and compound middle lamellae. For example, the longitudinal tracheid indicated by the arrow (85-min specimen) in Fig. 9 had a relatively higher WPG_{CW} in the compound middle lamella than in the secondary cell wall layers. Although it could not be for certain that the compound middle lamella regions of the sections were not thicker, the observed increased infiltration is supported by considering that the middle lamella does not have the chemically inaccessible cellulose elementary fibrils like the secondary cell wall layers [46]. The middle lamella also appeared to provide some barrier to BrPF infiltration between longitudinal tracheids. For example, near the middle lamella on the right-hand side of the indicated longitudinal tracheid (85-min specimen) in Fig. 9, the secondary cell wall layers' WPG_{CW} was higher in the indicated longitudinal tracheid to which the BrPF flowed than in its neighboring longitudinal tracheid.

The bondlines in Figs. 8 and 9 also show that the extent of BrPF infiltration did not extend beyond the cell neighboring the cell to which the resin flowed and the infiltration initiated. These initiation points included the application surface and micron-scale voids in the wood structure through which the BrPF flowed, such as the ray cells, pits, and longitudinal tracheid lumina. This limited extent of infiltration

from where the resin flowed suggests that for these resins, the size of the adhesive interphase can be approximately quantified using the flow quantification, such as the WP measurements in Fig. 7. The amount of cell wall infiltration depended on how many infiltration points were in the immediate vicinity of the cell wall. For example, again using the longitudinal tracheid indicated by the arrow (85-min specimen) in Fig. 9, this longitudinal tracheid has a filled lumen and would be expected to have concentric cell wall infiltration. However, below this marked longitudinal tracheid is another longitudinal tracheid with a filled lumen, and in the lower cell wall of the indicated tracheid the WPG_{CW} was higher because of the additive effect of the BrPF infiltrating from both of the lumina. Similarly, at the left-hand side of the marked longitudinal tracheid is a ray cell, and the left-hand secondary cell walls also have higher BrPF WPG_{CW} because of the addition of the BrPF infiltrating from the ray. The small extent of infiltration beyond the cell to which the resin flowed indicates that in order to infiltrate and modify the properties of multiple layers of cells near a bondline, adhesive flow into these cells is also needed.

Thus far, we have separated adhesive penetration only into flow and infiltration. However, many studies suggest that not all adhesive infiltration is equivalent. For example, Laborie and coworkers infiltrated wood with a low M_W PF and a high M_W PF that had a small fraction of a low M_W PF component [47]. They found that the low M_W fraction of their high M_W PF acted to plasticize lignin inside wood cell walls, whereas wood treated with only the low M_W PF did not plasticize the lignin. In our prior study using the same BrPF bondlines presented in this paper, we utilized nanoindentation to assess the hygromechanical properties of the infiltrated wood cell walls [24]. It was found that for a given amount of BrPF infiltration, the lower M_W BrPFs were more effective at minimizing mechanical softening caused by high relative humidity. Plaza and coworkers working with deuterium-labeled PF have also found it possible for PF to infiltrate the space between cellulose elementary fibrils within the microfibril [25, 26]. These results suggest that, in addition to quantifying adhesive flow and infiltration into wood as presented here, the nano- and molecular-scale interactions between the infiltrating adhesive and wood also need to be taken into consideration. Therefore, in addition to the micron- and molecular-

scale Norimoto models for chemical–wood interactions [48], results from this study and the recently proposed nanoscale models for chemical–wood interactions [49] should also be useful to aid and build understandings of adhesive performance.

Concluding remarks

X-ray computed tomography and XFM techniques have been employed to observe and quantify the flow and infiltration of BrPF into latewood loblolly pine. The efficacy of the techniques was demonstrated using bondlines made with latewood loblolly pine and BrPF resins with different M_w . It was shown how XCT can be used to quantify adhesive flow as a function of distance from the bondline and parameterized by calculating WP values. In future work, this will be useful in combination with adhesive performance studies to determine the extent of adhesive flow needed to obtain desired bondline performance. X-ray fluorescence microscopy was used to map BrPF infiltration pathways into wood cell walls, and protocols were developed to quantify the BrPF WPG_{CW}. Following this work, XFM will be useful in studies to determine the amount of infiltration needed to obtain cell walls with properties that lead to optimal bondline performance. Although much additional work is needed, the new insights gained and characterization tools developed in this study will be useful in the development of improved models capable of predicting adhesive bondline performance. These models should improve upon those classically put forward by Marra [4] and accelerate the development of improved engineered wood products that rely on adhesives.

Acknowledgements

This research used resources of the Advanced Photon Source, a US Department of Energy (DOE) Office of Science User Facility operated for the DOE Office of Science by Argonne National Laboratory under Contract No. DE-AC02-06CH11357.

Compliance with the ethical standards

Conflict of interest The authors declare that they have no conflict of interest.

Electronic supplementary material: The online version of this article (<https://doi.org/10.1007/s10853-018-2783-5>) contains supplementary material, which is available to authorized users.

References

- [1] ASTM International (2007) ASTM adhesives standards, vol 1506. ASTM International, Conshohocken
- [2] Frihart CR (2005) Wood adhesion and adhesives. In: Rowell RM (ed) Handbook of wood chemistry and wood composites, 2nd edn. Taylor & Francis, New York, pp 215–278
- [3] Kamke FA, Lee JN (2007) Adhesive penetration in wood—a review. *Wood Fiber Sci* 39:205–220
- [4] Marra AA (1992) Technology of wood bonding: principles in practice. Springer, New York
- [5] Frihart CR (2009) Adhesive groups and how they relate to the durability of bonded wood. *J Adhes Sci Technol* 23:611–627
- [6] Nearn W (1965) Wood-adhesive interface relations. *Off Dig Fed Soc Paint Technol* 37:720–733
- [7] Nearn WT (1974) Application of the ultrastructure concept in industrial wood products research. *Off Dig Fed Soc Paint Technol* 6:285–293
- [8] Wimmer R, Kläusler O, Niemz P (2013) Water sorption mechanisms of commercial wood adhesive films. *Wood Sci Technol* 47:763–775
- [9] Glass SV, Zelinka SL (2010) Moisture relations and physical properties of wood. In: Wood handbook: wood as an engineering material, Centennial edn. General technical report FPL, GTR-190. U.S. Dept. of Agriculture, Forest Service, Forest Products Laboratory, Madison, pp 4.1–4.19
- [10] Konnerth J, Gindl W (2006) Mechanical characterisation of wood-adhesive interphase cell walls by nanoindentation. *Holzforschung* 60:429–433
- [11] Modzel G, Kamke FA, De Carlo F (2011) Comparative analysis of a wood: adhesive bondline. *Wood Sci Technol* 45:147–158
- [12] Gardner DJ, Blumentritt M, Wang L, Yildirim N (2015) Adhesion theories in wood adhesive bonding. In: Mittal KL (ed) Progress in adhesion and adhesives. Wiley, Hoboken, pp 125–168
- [13] Frazier CE, Ni J (1998) On the occurrence of network interpenetration in the wood–isocyanate adhesive interphase. *Int J Adhes Adhes* 18:81–87
- [14] Gindl W, Dessipri E, Wimmer R (2002) Using UV-microscopy to study diffusion of melamine–urea–formaldehyde resin in cell walls of spruce wood. *Holzforschung* 56:103–107

- [15] Furuno T, Imamura Y, Kajita H (2004) The modification of wood by treatment with low molecular weight phenol-formaldehyde resin: a properties enhancement with neutralized phenolic-resin and resin penetration into wood cell walls. *Wood Sci Technol* 37:349–361
- [16] Konnerth J, Harper D, Lee S-H et al (2008) Adhesive penetration of wood cell walls investigated by scanning thermal microscopy (SThM). *Holzforchung* 62:91–98
- [17] Xu D, Zhang Y, Zhou H et al (2016) Characterization of adhesive penetration in wood bond by means of scanning thermal microscopy (SThM). *Holzforchung* 70:323–330
- [18] Xing C, Riedl B, Cloutier A, Shaler SM (2005) Characterization of urea-formaldehyde resin penetration into medium density fiberboard fibers. *Wood Sci Technol* 39:374–384
- [19] Cyr P-L, Riedl B, Wang X-M (2008) Investigation of urea-melamine-formaldehyde (UMF) resin penetration in medium-density fiberboard (MDF) by high resolution confocal laser scanning microscopy. *Holz Roh Werkst* 66:129–134
- [20] Hunt CE, Jakes JE, Grigsby W (2010) Evaluation of adhesive penetration of wood fibre by nanoindentation and microscopy. In: *BIOCOMP 2010; 10th Pacific Rim bio-based composites symposium*, pp 216–226
- [21] Grigsby WJ, Thumm A (2012) Resin and wax distribution and mobility during medium density fibreboard manufacture. *Eur J Wood Wood Prod* 70:337–348
- [22] Wang X, Deng Y, Li Y et al (2016) In situ identification of the molecular-scale interactions of phenol-formaldehyde resin and wood cell walls using infrared nanospectroscopy. *RSC Adv* 6:76318–76324
- [23] Jakes JE, Gleber S-C, Vogt S et al (2013) New synchrotron-based technique to map adhesive infiltration in wood cell walls. In: *Proceedings of 2013 annual meeting of the Adhesion Society, Daytona Beach Ocean, Resort Daytona Beach, FL, Daytona Beach, FL, USA, 3–6 Mar 2013*, pp 1–3
- [24] Jakes JE, Hunt CG, Yelle DJ et al (2015) Synchrotron-based X-ray fluorescence microscopy in conjunction with nanoindentation to study molecular-scale interactions of phenol-formaldehyde in wood cell walls. *ACS Appl Mater Interfaces* 7:6584–6589
- [25] Plaza NZ (2017) Neutron scattering studies of nano-scale wood-water interactions. PhD dissertation, University of Wisconsin-Madison
- [26] Plaza NZ, Frihart CR, Hunt CG et al (2017) Small angle neutron scattering as a new tool to study moisture-induced swelling in the nanostructure of chemically modified wood cell walls. In: *Hunt CG, Smith GD, Yan N (eds) Proceedings of the international conference on wood adhesives 2017*. Forest Products Society, Peachtree Corners, GA
- [27] Evans PD, Morrison O, Senden TJ et al (2010) Visualization and numerical analysis of adhesive distribution in particleboard using X-ray micro-computed tomography. *Int J Adhes Adhes* 30:754–762
- [28] Paris JL, Kamke FA (2015) Quantitative wood-adhesive penetration with X-ray computed tomography. *Int J Adhes Adhes* 61:71–80
- [29] Hansen CM, Bjorkman A (1998) Ultrastructure of wood from a solubility parameter point of view. *Holzforchung* 52:335–344
- [30] Mantanis GI, Young RA, Rowell RM (1994) Swelling of wood. Part II. Swelling in organic liquids. *Holzforchung* 48:480–490
- [31] Gürsoy D, De CF, Xiao X (2014) TomoPy: a framework for the analysis of synchrotron tomographic data. *J Synchrotron Radiat* 21:118–1193
- [32] McKinley PE, Ching DJ, Kamke FA et al (2016) Micro X-ray computed tomography of adhesive bonds in wood. *Wood Fiber Sci* 48:2–16
- [33] Schmid B, Schindelin J, Cardona A et al (2010) A high-level 3D visualization API for Java and ImageJ. *BMC Bioinformatics* 11:274. <https://doi.org/10.1186/1471-2105-11-274>
- [34] Schindelin J, Arganda-Carreras I, Frise E et al (2012) Fiji: an open-source platform for biological-image analysis. *Nat Methods* 9:676–682
- [35] Vogt S (2003) MAPS: a set of software tools for analysis and visualization of 3D X-ray fluorescence data sets. *J Phys IV* 104:635–638
- [36] Paris JL, Kamke FA, Mbachu R, Gibson SK (2014) Phenol formaldehyde adhesives formulated for advanced X-ray imaging in wood-composite bondlines. *J Mater Sci* 49:580–591. <https://doi.org/10.1007/s10853-013-7738-2>
- [37] Paris JL, Kamke FA, Xiao X (2015) X-ray computed tomography of wood-adhesive bondlines: attenuation and phase-contrast effects. *Wood Sci Technol* 49:1185–1208
- [38] Dunky M (2003) Adhesives in the wood industry. In: *Pizzi A, Mittal K (eds) Handbook of adhesive technology, revised and expanded, 2nd edn*. CRC Press, Boca Raton, pp 887–956
- [39] Hass P, Wittel FK, Mendoza M et al (2012) Adhesive penetration in beech wood: experiments. *Wood Sci Technol* 46:243–256
- [40] Sernek M, Resnik J, Kamke FA (1999) Penetration of liquid urea-formaldehyde adhesive into beech wood. *Wood Fiber Sci* 31:41–48
- [41] Tarkow H, Feist WC, Southerland CF (1966) Interaction of wood with polymeric materials—penetration versus molecular size. *For Prod J* 16:61–65
- [42] Thybring EE, Kymäläinen M, Rautkari L (2018) Experimental techniques for characterising water in wood covering the range from dry to fully water-saturated. *Wood Sci Technol* 52:297–329

- [43] Hunt C, O'Dell J, Jakes J et al (2015) Wood as polar size exclusion chromatography media: implications to adhesive performance. *For Prod J* 65:9–14
- [44] Gabrielli CP, Kamke FA (2009) Phenol-formaldehyde impregnation of densified wood for improved dimensional stability. *Wood Sci Technol* 44:95–104
- [45] Stamm AJ, Seborg RM (1936) Minimizing wood shrinkage and swelling. *Ind Eng Chem* 28:1164–1169
- [46] Rowell RM, Petterson R, Tshabalala MA (2013) Cell wall chemistry. In: Rowell RM (ed) *Handbook of wood chemistry and wood composites*, 2nd edn. Taylor & Francis, New York, pp 33–72
- [47] Laborie M-PG, Salmen L, Frazier CE (2006) A morphological study of the wood/phenol-formaldehyde adhesive interphase. *J Adhes Sci Technol* 20:729–741
- [48] Norimoto M (2001) Chemical modification of wood. In: Hon DN-S, Shirashi N (eds) *Wood and cellulose chemistry*, 2nd edn. Marcel Dekker, New York, pp 573–598
- [49] Jakes JE, Frihart CR, Hunt CG et al (2017) Integrating multi-scale studies of adhesive penetration into wood. In: Hunt CG, Smith GD, Yan N (eds) *Proceedings of the international conference on wood adhesives 2017*. Forest Products Society, Peachtree Corners, GA